hp-adaptive discontinuous Galerkin methods for bifurcation phenomena in open flows

CrossMark

K.A. Cliffe, E.J.C. Hall, P. Houston *

School of Mathematical Sciences, University of Nottingham, University Park, Nottingham NG7 2RD, UK

ARTICLE INFO

ABSTRACT

We consider the application of high-order/*hp*-version adaptive discontinuous Galerkin finite element methods for the discretization of the bifurcation problem associated with the steady incompressible Navier–Stokes equations. Based on exploiting the Dual Weighted Residual approach, reliable and efficient *a posteriori* estimates of the error in the computed critical Reynolds number at which a steady pitchfork bifurcation occurs when the underlying physical system possesses either reflectional Z_2 symmetry, or rotational and reflectional $O(2)$ symmetry, are derived. Numerical experiments highlighting the practical performance of the proposed *a posteriori* error indicator on *hp*-adaptively refined computational meshes are presented for both two- and three-dimensional problems.

1. Introduction

The purpose of this article is to consider the application of *hp*-version adaptive discontinuous Galerkin finite element methods (DGFEMs) to bifurcation problems. In particular, we study the linear stability of the two- and three-dimensional incompressible Navier–Stokes equations in the case when the underlying system possesses either reflectional Z_2 symmetry or both rotational and reflectional $O(2)$ symmetry, respectively. Here, the key objective is to adaptively construct sequences of *hp*-finite element spaces in order to accurately and reliably compute the critical Reynolds number Re^c at which a (steady) bifurcation point first occurs, cf. the review article [1], and the references cited therein. For simplicity, we assume that a symmetric steady state solution to the incompressible Navier–Stokes equations undergoes a steady pitchfork bifurcation at the critical value Re^c; we point out that Hopf bifurcations may also be treated within a similar framework, cf. [2], and the references cited therein. In order to estimate the critical Re^c, the approach adopted within this article is to consider the construction and subsequent DGFEM approximation of a suitable extended system of partial differential equations, which must be solved for the underlying flow variables, the corresponding null solution, and Re^c; for details, see [3,4] for steady bifurcations. The *hp*-version of the DGFEM is based on exploiting a (symmetric) interior penalty discretization of the second-order viscous terms, together with an upwind treatment of the nonlinear transport operator; cf. [5–7]. This discretization approach is advantageous both from the point of view of ease of *hp*-adaptivity and stability of the underlying scheme at high Reynolds numbers. The proposed *hp*-adaptive algorithm is based on exploiting the Dual Weighted Residual (DWR) *a posteriori* error estimation technique, cf. [8] and the references cited therein, to estimate the error in the critical parameter of interest, namely Re^c. The numerical performance of the error estimation techniques developed in this article for computing steady pitchfork bifurcations, as well as the computational efficiency of exploiting *hp*-mesh adaptation for determining flow stability will be investigated. The work presented in this article is a complete and improved account of our recent work announced in the conference article [9]. To the best of our knowledge, this article and [9] represent the first attempt

---

* Corresponding author.
E-mail addresses: Andrew.Cliffe@nottingham.ac.uk (K.A. Cliffe), Edward.Hall@nottingham.ac.uk (E.J.C. Hall), Paul.Houston@nottingham.ac.uk (P. Houston).

to apply *hp*-adaptive DGFEMs to study the linear stability of incompressible fluid flows. For the application of standard *h*-version adaptive finite element methods to bifurcation problems, we refer to our earlier work in the articles [10,2,11].

The paper is structured as follows. In Section 2 we consider the construction of the above-mentioned extended system for the detection of the location at which a bifurcation may occur from a steady state solution of an abstract time dependent problem. Then, in Section 3 we then show how we can utilize either Z_2 or $O(2)$ symmetry in the underlying problem to reduce the computational complexity. Section 4 is devoted to the derivation of a goal-oriented *a posteriori* estimate for the error between the true value of the critical parameter and the computed one, when a general finite element method is employed. In Section 5 we investigate the practical performance of the proposed *a posteriori* error estimator on sequences of *hp*-adaptively generated meshes for three standard test problems. Here, the quality of the computed *a posteriori* error estimate is studied; moreover, comparisons between the exploitation of *h*- and *hp*-refinement strategies are reported. We then apply the techniques developed in this article to the problem of a sudden expansion in a cylindrical pipe. This represents a notoriously difficult computational problem; for related experimental work, we refer to [12]. Finally, we summarize the work presented in this article and draw some conclusions in Section 6.

2. Detecting steady bifurcation points

In this section, we briefly outline the general mathematical framework for accurately locating the critical parameter value at which a bifurcation may occur from a steady state solution of an abstract time dependent problem. The simplification of the proposed extended system formulation when the underlying problem possesses either Z_2 or $O(2)$ symmetry will also be considered; the material presented here is based on the detailed discussion outlined in our recent articles [2,11]. To this end, given a map $F : V \times \mathbb{R} \to V$, where V is a Banach space with norm $\|\cdot\|$, consider the nonlinear time dependent problem

$$\frac{\partial u}{\partial t} + F(u, \lambda) = 0, \tag{1}$$

where λ is some parameter of interest and u is a state variable. For the purposes of this article, F will represent the incompressible Navier–Stokes equations posed in an open domain $\Omega \subset \mathbb{R}^d$, $d = 2, 3$, subject to appropriate boundary conditions, with V a subset of $H^1(\Omega)^d \times L_2(\Omega)$. Moreover, λ is identified as the Reynolds number *Re*.

One of the key objectives in computational bifurcation theory is to locate the critical parameter value λ^c at which solutions lose (linear) stability and bifurcations occur. To this end, we assume that F is a C^p, $p \geq 3$, mapping. We denote the Fréchet derivative of F with respect to u at a fixed point $(w, \chi) \in V \times \mathbb{R}$ by $F'_u(w, \chi; \cdot)$ and similarly the derivative with respect to λ by $F'_\lambda(w, \chi)$. We use the convention that in semi-linear forms such as $F'_u(\cdot, \cdot; \cdot)$ the form is linear with respect to all arguments to the right of the semicolon. We will assume that $F'_u(u, \lambda; \cdot) : V \to V$ is Fredholm of index 0 for all $(u, \lambda) \in V \times \mathbb{R}$. Higher order Fréchet derivatives are written in a similar manner; for example, the Fréchet derivative of $F'_u(w, \chi; \cdot)$ with respect to u acting on the function v is denoted by $F''_{uu}(w, \chi; \cdot, v)$.

Writing u_s to denote the steady state solution of the steady version of (1), i.e.,

$$F(u_s, \lambda) = 0, \tag{2}$$

the linear stability of u_s at specific parameter values λ may be determined by the nature of the eigenvalues μ of the corresponding eigenvalue problem:

$$F'_u(u_s, \lambda; \phi) = \mu\phi. \tag{3}$$

A change in sign of the real part of any of the eigenvalues from positive to negative indicates a loss of stability. If a single real-valued eigenvalue crosses the imaginary axis, then a steady bifurcation occurs; a complex conjugate pair of eigenvalues crossing the imaginary axis indicates the existence of a Hopf bifurcation, in which case a branch of time-periodic solutions emanates from the bifurcation point. For the purposes of this article we only consider steady bifurcations; see [13,2], where Hopf bifurcations are treated for Z_2-symmetric problems. The application of DWR *a posteriori* error estimation to accurately compute the eigenvalues μ for a series of parameter values λ has been considered in [13], for example; for the error estimation of the computed *critical parameter value*, *i.e.*, the value where the steady solution first loses linear stability, we refer to [10,2,11]. This latter setting is the focus of the current article.

With this in mind, we seek to directly determine the critical parameter value which has an eigenvalue with zero real part. On the basis of Eqs. (2)–(3) the following extended system formulation may be considered: find $\mathbf{u} := (u, \phi, \lambda)$ such that

$$T(\mathbf{u}) \equiv \begin{pmatrix} F(u, \lambda) \\ F'_u(u, \lambda; \phi) \\ \langle \phi, g \rangle - 1 \end{pmatrix} = \mathbf{0}, \tag{4}$$

where we have dropped the subscript "*s*" for notational simplicity. Here, $\langle \cdot, \cdot \rangle$ denotes the duality pairing between the spaces V and V', V' being the dual space of V, and $g \in V'$ is some suitable functional satisfying $\langle \phi, g \rangle \neq 0$.

In the following section, we discuss how the complexity of the extended system (4) may be reduced when the given problem possesses an underlying symmetry structure; for further details, see [2,11], for the case of Z_2 and $O(2)$ symmetry, respectively.

3. Bifurcation in the presence of symmetry

In principal the extended system (4) may be directly discretized in order to compute a numerical approximation of the critical value λ^c of the parameter of interest. However, in order to render (4) computationally tractable, so that accurate and reliable *mesh independent* predictions of λ^c may be computed, it is desirable to first reduce the complexity of (4) when the problem at hand possesses an underlying symmetry; see [14–16], for example. The key idea is that under the action of a group $\mathcal{G}$, the Jacobian of a nonlinear problem may be simplified, subject to the selection of an appropriate basis, thereby leading to computational savings.

Throughout this section, we assume that $\mathcal{G}$ is a given (symmetry) group. $\mathcal{G}$ acts (linearly) on V if there exists a continuous mapping $\mathcal{G} \times V \to V$ given by $(\gamma, u) \mapsto \gamma u, u \in V$, which satisfies:

(a) For every $\gamma \in \mathcal{G}$ the mapping $\rho_\gamma : V \to V$, defined by $\rho_\gamma u := \gamma u, u \in V$, is linear.
(b) If $\gamma_1, \gamma_2 \in \mathcal{G}$ then $(\gamma_1 \gamma_2) u = \gamma_1 (\gamma_2 u)$ for all $u \in V$.

The mapping ρ that takes $\gamma \in \mathcal{G}$ to ρ_γ is called the representation of $\mathcal{G}$ on V.

Consider the steady variant of problem (1): find u such that

$$F(u, \lambda) = 0,$$

where additionally we assume that F is $\mathcal{G}$ equivariant. By this we mean that

$$\rho_\gamma F(u, \lambda) = F(\rho_\gamma u, \lambda) \tag{5}$$

$\forall \gamma \in \mathcal{G}$ and $u \in V$. The equivariance condition (5) implies that, if u is a solution of $F(u, \lambda) = 0$, then for any $\gamma \in \mathcal{G}$, $\rho_\gamma u$ is also a solution. A subspace $\mathcal{S} \subset V$ is referred to as being $\mathcal{G}$ invariant if for all $\gamma \in \mathcal{G}$, $\rho_\gamma : \mathcal{S} \to \mathcal{S}$.

We are primarily interested in bifurcations away from paths of steady $\mathcal{G}$ symmetric solutions and define the symmetric subspace $V^{\mathcal{G}}$ of V by

$$V^{\mathcal{G}} := \{v \in V : \rho_\gamma v = v\},$$

for $\gamma \in \mathcal{G}$. From (5) we deduce that $V^{\mathcal{G}}$ is invariant under F, if F is $\mathcal{G}$ equivariant. Writing $F^{\mathcal{G}}$ to denote the restriction of F to $V^{\mathcal{G}}$, steady $\mathcal{G}$ symmetric solutions of (1) may be determined from the reduced problem

$$F^{\mathcal{G}}(u, \lambda) = 0, \quad u \in V^{\mathcal{G}}. \tag{6}$$

Taking the Fréchet derivative of (5) with respect to u gives

$$\rho_\gamma F_u'(u, \lambda; \phi) = F_u'(\rho_\gamma u, \lambda; \rho_\gamma \phi) \quad \forall \phi \in V.$$

Hence, if $u \in V^{\mathcal{G}}$, then we have

$$\rho_\gamma F_u'(u, \lambda; \phi) = F_u'(u, \lambda; \rho_\gamma \phi) \quad \forall \phi \in V.$$

In the case when $u \in V^{\mathcal{G}}$, we note that $F_u'(u, \lambda; \cdot)$ is also $\mathcal{G}$ equivariant. With these observations, in the following two sections we discuss the specific cases when $\mathcal{G} = Z_2$ and $\mathcal{G} = O(2)$, respectively.

3.1. Bifurcation in the presence of Z_2 symmetry

In this section, we consider the computation of steady pitchfork bifurcations in the case when the underlying problem possesses Z_2 symmetry; for the treatment of Hopf bifurcations in this setting, we refer to [2] and the references cited therein. To this end, we write $Z_2 = \{I, s\}$ to denote the simplest symmetry group, where I denotes the group identity operator and s is a reflection, satisfying $s^2 = I$.

Thereby, the symmetric subspace V^s of V is given by

$$V^{Z_2} \equiv V^s := \{v \in V : \rho_s v = v\},$$

where ρ_s is the representation of the reflection $s \in Z_2$. Similarly, $V^a := \{v \in V : \rho_s v = -v\}$ denotes the antisymmetric subspace V^a of V; thereby, we may write $V = V^s \oplus V^a$.

To reduce the complexity of the underlying bifurcation problem, we note that: given a Z_2 equivariant linear operator $A : V \to V$, the spaces $V^\sigma, \sigma = s, a$, are invariant subspaces of A, i.e., $A : V^\sigma \to V^\sigma, \sigma = s, a$, respectively; cf. [17]. This leads to the Jacobian operator $F_u'(u, \lambda; \cdot)$, for $u \in V^s$, having a diagonal block structure, cf. above. This is formally encapsulated in the following result.

Lemma 1. *Suppose that $u \in V^s$ and μ is an eigenvalue of*

$$F_u'(u, \lambda; \phi) = \mu \phi, \quad \phi \in V,$$

then either $\phi \in V^s$, or else $\phi \in V^a$.

Lemma 1 states that the Z_2 symmetry present in the underlying problem implies that the eigenvectors are either symmetric or else antisymmetric. Indeed, at a bifurcation point, the null solution will be either symmetric or antisymmetric; if the null solution is symmetric, all the solutions locally lie in V^s and one would typically observe a limit point bifurcation. In this article, we are interested in the case when a symmetry breaking bifurcation arises, i.e., when $\phi \in V^a$. Hence, we can locate critical parameter values at which symmetric steady state solutions $u \in V^s$ lose stability, by solving the following problem. For a steady bifurcation, find $\mathbf{u} = (u, \phi, \lambda) \in V^s \times V^a \times \mathbb{R}$ such that

$$T(\mathbf{u}) \equiv \begin{pmatrix} F(u, \lambda) \\ F'_u(u, \lambda; \phi) \\ \langle \phi, g \rangle - 1 \end{pmatrix} = \mathbf{0}, \tag{7}$$

where $g \in (V^a)'$ is some suitable functional satisfying $\langle \phi, g \rangle \neq 0$. In addition, we assume that we have a pitchfork bifurcation, in which case the following condition also holds

$$\langle F''_{u\lambda}(u, \lambda; \phi) + F''_{uu}(u, \lambda; w, \phi), \varrho \rangle \neq 0, \tag{8}$$

where $\varrho \in \ker(F^*_u)$, F^*_u denotes the adjoint of $F'_u(u, \lambda, \cdot)$, and $w \in V^s$ solves $F'_u(u, \lambda; w) + F'_\lambda(u, \lambda) = 0$. Eq. (8) is the standard non-degeneracy condition that holds at a pitchfork bifurcation; for further details, we refer to [18,14].

3.2. Bifurcation in the presence of $O(2)$ symmetry

We now consider the case when the underlying problem possesses both rotational and reflectional, i.e., $O(2)$ symmetry. To this end, we note that $O(2)$ is the Lie group which comprises rotations r_α, $\alpha \in \mathbb{R}$, and a reflection s, cf. [11]. In the $O(2)$ case, there exists a unique orthogonal decomposition of V, given by

$$V = \sum_{m=0}^{\infty} V^m, \quad V^m \perp V^l, m \neq l, \tag{9}$$

where each V^m is an irreducible $O(2)$ invariant subspace of V, cf. [17]. In order to reduce the complexity of the underlying bifurcation problem, we note that given an $O(2)$ equivariant operator $A : V \to V$, then V^m are invariant under the action of A, i.e., $A : V^m \to V^m$, $m = 0, 1, 2, \ldots$, cf. [17].

The decomposition (9) is produced by the rotation elements r_α of $O(2)$; by exploiting the reflection s, each subspace V^m may be decomposed as

$$V^m = V^{m,s} \oplus V^{m,a}, \quad m = 1, 2, \ldots,$$

where $V^{m,s}$ and $V^{m,a}$ are the symmetric and anti-symmetric components of V^m, respectively, cf. Section 3.1.

With this notation, it can be shown (see [11,1] for details) that the critical parameter values at which symmetric steady state solutions $u \in V^{O(2)}$ lose stability may be located by solving the following problems for $m = 0, 1, \ldots$: find $\mathbf{u} = (u, \phi, \lambda) \in V^{O(2)} \times V^{m,\sigma} \times \mathbb{R}$ such that

$$T(\mathbf{u}) \equiv \begin{pmatrix} F(u, \lambda) \\ F'_u(u, \lambda; \phi) \\ \langle \phi, g \rangle - 1 \end{pmatrix} = \mathbf{0}, \tag{10}$$

where, for $m \geq 1$, $\sigma = s$ or $\sigma = a$ (both cases are equivalent in this setting), for $m = 0$, ϕ is sought in $V^0 = V^{O(2)}$, and $g \in V'$ is some suitable functional satisfying $\langle \phi, g \rangle \neq 0$. We emphasize that the key result is that the original problem can be divided up into a series of problems with reduced complexity. In particular, we point out that in the case when F represents the three-dimensional incompressible Navier–Stokes equations, written in cylindrical coordinates, the extended system (10) only requires the numerical solution of a series of two-dimensional problems in order to compute the critical Re at which the original three-dimensional problem loses linear stability; clearly, this leads to an enormous saving in computational costs, cf. [11,1]. For the purposes of this article we shall assume the physically more interesting case where the steady state solutions first become unstable with $m \neq 0$, in which case there is a symmetry breaking bifurcation; the case when $m = 0$ corresponds to a turning point or fold point. Furthermore, we assume that we have a bifurcation of pitchfork type, cf. below; here (u^0, λ^0) denotes the bifurcation point.

Theorem 1. *Let* $u(\lambda^0) = u^0 \in V^{O(2)}$. *Suppose that*

$$\text{Null}(F^0_u(\cdot)) \subset V^{m,s}, \quad m \neq 0,$$

where $F^0_u(\cdot) := F'(u^0, \lambda^0; \cdot)$, *and* $\mu = 0$ *is a simple eigenvalue, i.e.,*

$$\dim(\text{Null}(F^0_u(\cdot) \cap V^{m,s})) = 1 \quad \text{and} \quad \dim(\text{Null}(F^0_u(\cdot) \cap V^{m,a})) = 1.$$

Finally, let

$$b_\lambda := \langle F''_{u\lambda}(u, \lambda; \phi) + F''_{uu}(u, \lambda; w, \phi), \psi \rangle \neq 0, \tag{11}$$

where $\psi \in \ker(F^*_u)$ *for* F^*_u *the adjoint of* $F'_u(u, \lambda, \cdot)$ *and* $w \in V^{m,s}$ *solves* $F'_u(u, \lambda; w) + F'_\lambda(u, \lambda) = 0$.

Then there exists a secondary branch of $O(2)$ symmetry breaking solutions. The bifurcation is of pitchfork type and the bifurcating branch has D_m symmetry. Here, D_m is the dihedral group generated by $r_{2\pi/m}$ and s.

Proof. For details, we refer to [1], and the references cited therein. $\quad\square$

4. *A posteriori* error estimation

In this section, we consider the derivation of a goal-oriented *a posteriori* estimate for the error in the computed critical parameter when the extended systems (7) and (10) are numerically approximated by a general Galerkin finite element method. To this end, we write $\mathbf{V}_{Z_2} = V^s \times V^a \times \mathbb{R}$ and $\mathbf{V}_{O(2),m} = V^{O(2)} \times V^{m,s} \times \mathbb{R}$, $m = 1, 2, \ldots$. For the computational examples presented in Section 5 which possess $O(2)$ symmetry, namely, those presented in Sections 5.2–5.4, the critical azimuthal wave number is $m = 1$; with this in mind, we use the shorthand notation $\mathbf{V}_{O(2)} = \mathbf{V}_{O(2),1}$. Thereby, the extended systems (7) and (10) may be written in the following compact form: find $\mathbf{u} \in \mathbf{V}_\mathscr{S}$ such that

$$T(\mathbf{u}) = \mathbf{0}, \tag{12}$$

where $\mathscr{S} = Z_2$ when the underlying problem exhibits Z_2 symmetry, and $\mathscr{S} = O(2)$ for $O(2)$ symmetric bifurcation problems. We remark that the precise definition of the operator T depends on both the underlying physical system under consideration (in our case the incompressible Navier–Stokes equations in two- or three-dimensions), as well as the symmetry properties present in the underlying bifurcation problem (i.e., for the purposes of this article, Z_2 or $O(2)$). The precise definition of T for two-dimensional incompressible fluid flows in the Z_2 setting is presented in [2]; see [11] for the definition of T when the underlying PDE problem is the three-dimensional incompressible Navier–Stokes equations, written in cylindrical coordinates, when the underlying system possesses $O(2)$ symmetry. For brevity, these details are omitted.

We begin by first introducing a suitable finite element approximation of the bifurcation problem (12). To this end, we consider a sequence of finite element spaces $\mathbf{V}_{\mathscr{S},h,\mathbf{p}}$, $\mathscr{S} = Z_2, O(2)$, consisting of (discontinuous) piecewise polynomial functions of composite degree $\mathbf{p}$ on a partition $\mathcal{T}_h = \{\kappa\}$ of granularity h, from which we shall approximate the steady solution $\mathbf{u}$. In particular, we allow the polynomial degree vector $\mathbf{p}$ to vary from element to element.

We find the triple $\mathbf{u}_h = (u_h, \phi_h, \lambda_h) \in \mathbf{V}_{\mathscr{S},h,\mathbf{p}}$, $\mathscr{S} = Z_2, O(2)$, such that

$$\mathcal{N}(\mathbf{u}_h; \mathbf{v}_h) := \hat{\mathcal{N}}(u_h, \lambda_h; v_h) + \hat{\mathcal{N}}'_u(u_h, \lambda_h; \phi_h, \varphi_h) + \chi_h((g, \phi_h) - 1) = 0 \quad \forall \mathbf{v}_h \in \mathbf{V}_{\mathscr{S},h,\mathbf{p}}, \tag{13}$$

where $\mathbf{v}_h := (v_h, \varphi_h, \chi_h)$, $(\cdot, \cdot)$ denotes the standard L^2-inner product, $\hat{\mathcal{N}}(\cdot, \cdot; \cdot)$ is the semi-linear form associated with the discretization of the underlying steady state version of the partial differential equation (1) and $\hat{\mathcal{N}}'_u(\cdot, \cdot; \cdot, \cdot)$ is the Jacobian of $\hat{\mathcal{N}}(\cdot, \cdot; \cdot)$ with respect to u and thus represents the discretization of $F'_u(\cdot, \cdot; \cdot)$. For the numerical experiments presented in Section 5, this discretization is based on employing the (symmetric) version of the interior penalty discontinuous Galerkin method, together with a Lax–Friedrichs numerical flux approximation of the nonlinear convective terms. In particular, we employ mixed-order spaces of discontinuous piecewise polynomials for the approximation of the velocity and pressure variables present in both the state variable and null function; for complete details of this numerical scheme, we refer to the articles [2,11] for the two cases when $\mathscr{S} = Z_2, O(2)$, respectively; again, for brevity, the details are omitted.

Here, we assume that the finite element method (13) is consistent, i.e.,

$$\mathcal{N}(\mathbf{u}, \mathbf{v}_h) = 0 \quad \forall \mathbf{v}_h \in \mathbf{V}_{\mathscr{S},h,\mathbf{p}}, \tag{14}$$

where $\mathscr{S} = Z_2, O(2)$ and $\mathbf{u}$ denotes the analytical solution of (12).

For the linear target functional of practical interest $J(\mathbf{u}) = \lambda$, we outline the DWR technique, cf. [8], for estimating the approximation error $J(\mathbf{u}) - J(\mathbf{u}_h) \equiv \lambda - \lambda_h$. We write $\mathcal{M}(\cdot, \cdot; \cdot, \cdot)$ to denote the mean value linearization of $\mathcal{N}(\cdot; \cdot)$, defined by

$$\mathcal{M}(\mathbf{u}, \mathbf{u}_h; \mathbf{u} - \mathbf{u}_h, \mathbf{w}) = \mathcal{N}(\mathbf{u}; \mathbf{w}) - \mathcal{N}(\mathbf{u}_h; \mathbf{w})$$
$$= \int_0^1 \mathcal{N}'_{\mathbf{u}}(\theta\mathbf{u} + (1-\theta)\mathbf{u}_h; \mathbf{u} - \mathbf{u}_h, \mathbf{w}) \, d\theta, \tag{15}$$

for some $\mathbf{w} \in \hat{\mathbf{V}}_\mathscr{S}$, $\mathscr{S} = Z_2, O(2)$. Here, $\hat{\mathbf{V}}_\mathscr{S}$ is some suitably chosen space such that $\mathbf{V}_{\mathscr{S},h,\mathbf{p}} \subset \hat{\mathbf{V}}_\mathscr{S}$, $\mathscr{S} = Z_2, O(2)$, respectively. The formal *dual problem* is defined by: find $\mathbf{z} \in \hat{\mathbf{V}}_\mathscr{S}$, $\mathscr{S} = Z_2, O(2)$, such that

$$\mathcal{M}(\mathbf{u}, \mathbf{u}_h; \mathbf{w}, \mathbf{z}) = J(\mathbf{w}) \quad \forall \mathbf{w} \in \hat{\mathbf{V}}_\mathscr{S}. \tag{16}$$

Assuming that (16) is well-posed, exploiting the linearity of $J(\cdot)$, combining (15) and (16) and using the consistency condition (14) we deduce that

$$\lambda - \lambda_h = J(\mathbf{u}) - J(\mathbf{u}_h) = J(\mathbf{u} - \mathbf{u}_h) = \mathcal{M}(\mathbf{u}, \mathbf{u}_h; \mathbf{u} - \mathbf{u}_h, \mathbf{z})$$
$$= \mathcal{M}(\mathbf{u}, \mathbf{u}_h; \mathbf{u} - \mathbf{u}_h, \mathbf{z} - \bar{\mathbf{z}}_h)$$
$$= -\mathcal{N}(\mathbf{u}_h, \mathbf{z} - \bar{\mathbf{z}}_h) \quad \forall \bar{\mathbf{z}}_h \in \mathbf{V}_{\mathscr{S},h,\mathbf{p}}, \tag{17}$$
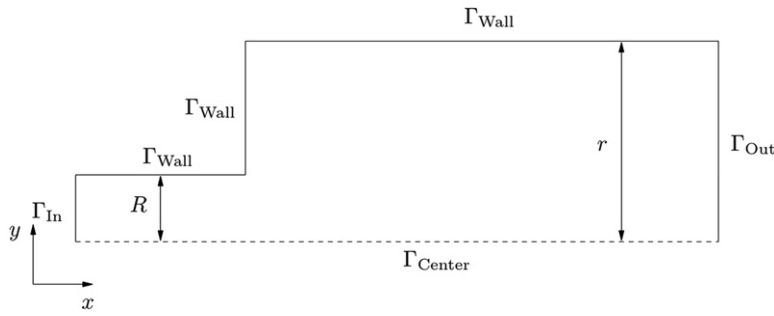
Fig. 1. 2D channel flow: half channel with a sudden expansion.

$\mathscr{S} = Z_2, O(2)$. For computational purposes, the error representation formula (17) must be numerically estimated by computing a suitable approximation $\mathbf{z}_h$ to the dual solution $\mathbf{z}$. To this end, we compute $\mathbf{z}_h \in \mathbf{V}_{\mathscr{S},h,\hat{\mathbf{p}}}$ using polynomials of degree $\hat{\mathbf{p}} > \mathbf{p}$ (understood elementwise) on the same finite element mesh $\mathcal{T}_h$ employed for the primal problem. Furthermore, we point out that the error representation formula (17) may be rewritten in the following equivalent elementwise form

$$\lambda - \lambda_h = \sum_{\kappa \in \mathcal{T}_h} \eta_\kappa;$$

here, $|\eta_\kappa|$ represent local elemental error indicators, which can be employed within an adaptive refinement strategy, cf. below. We remark that since DGFEMs satisfy the Galerkin orthogonality property elementwise, the element indicators $|\eta_k|$ are independent of the choice of $\bar{\mathbf{z}}_h$; indeed, here we simply select $\bar{\mathbf{z}}_h = \mathbf{0}$.

Given that the definition of the dual problem involves the unknown analytical solution $\mathbf{u}$, for computational purposes, a linearization error is committed; thereby, the numerical approximation of the dual problem is given by: find $\mathbf{z}_h := (z_u, z_\phi, z_\lambda) \in \mathbf{V}_{\mathscr{S},h,\hat{\mathbf{p}}}$, $\mathscr{S} = Z_2, O(2)$, such that

$$\hat{\mathcal{N}}_u'(u_h, \lambda_h; v_h, z_u) + \hat{\mathcal{N}}_\lambda'(u_h, \lambda_h; z_u)\chi_h + \hat{\mathcal{N}}_{uu}''(u_h, \lambda_h; \varphi_h, \phi_h, z_\phi) + \hat{\mathcal{N}}_u'(u_h, \lambda_h; \varphi_h, z_\phi)$$
$$+ \hat{\mathcal{N}}_{u\lambda}''(u_h, \lambda_h; \phi_h, z_\phi)\chi_h + z_\lambda(g, \varphi_h) = \chi_h \quad \forall \mathbf{v}_h \in \mathbf{V}_{\mathscr{S},h,\hat{\mathbf{p}}}, \tag{18}$$

where $\mathbf{v}_h := (v_h, \varphi_h, \chi_h)$.

5. Numerical experiments

In this section, we study the practical performance of the proposed *a posteriori* error estimator derived in Section 4 within an automatic *hp*-adaptive refinement procedure which is based on employing 1-irregular quadrilateral elements. Here, the elements are marked for refinement/derefinement on the basis of the size of the elemental error indicators $|\eta_\kappa|$, using the fixed fraction refinement algorithm with refinement and derefinement fractions set to 25% and 10%, respectively. Once an element $\kappa \in \mathcal{T}_h$ has been flagged for refinement, a decision must be made whether the local mesh size or the local degree of the approximating polynomial should be adjusted accordingly. The choice to perform either *h*- or *p*-refinement is based on estimating the local smoothness of the (unknown) analytical solution. To this end, we employ the *hp*-adaptive strategy developed in [19], where the local regularity of the analytical solution is estimated from truncated local Legendre expansions of the computed numerical solution. Throughout this section, the underlying linear systems are solved using the direct solver MUMPS, cf. [20–22].

5.1. Flow in a channel with a sudden expansion

In this first example we consider the flow of an incompressible fluid in a two-dimensional channel with a sudden expansion. Writing R and r to denote the radius of the inlet section of the channel and the radius of the main part of the channel, respectively, we set $r : R = 3 : 1$, see Fig. 1. At the inflow, Γ_{In}, the flow is assumed to be Poiseuille; no slip Dirichlet conditions are imposed on Γ_{Wall}, a Neumann condition is enforced on Γ_{Out} and a mixed boundary condition is imposed on Γ_{Center}.

With this configuration, it is well known, see [23], for example, that there exists a steady Z_2 symmetry breaking pitchfork bifurcation, where a real eigenvalue crosses the imaginary axis at around $Re = 40$; computations on very fine meshes predict that $Re^c \approx 40.5578770$, cf. [2]. In Table 1 we present the performance of our adaptive algorithm based on employing 11 *hp*-refinements. Here, we show the number of elements, the number of degrees of freedom in computing the primal base solution and the primal null function, the error in the critical Reynolds number and the effectivities $\tau = |\sum_{\kappa \in \mathcal{T}_h} \eta_\kappa| / |Re^c - Re_h^c|$. We notice immediately that, as the mesh is refined, the effectivities tend to unity, indicating that the computed error representation formula provides a reliable estimate of the discretization error in the computed critical *Re*.

Table 1
2D channel flow: *hp*-adaptive algorithm.

Eles	Base dof	Null dof	Re_h^c	$|Re^c - Re_h^c|$	τ
640	14,080	14,080	40.492306	6.553E−02	1.83
814	19,941	19,941	40.526208	3.163E−02	1.66
1093	29,346	29,346	40.543004	1.483E−02	1.64
1510	43,168	43,168	40.550875	6.960E−03	1.56
1924	59,180	59,180	40.554062	3.773E−03	1.40
2419	79,460	79,460	40.555699	2.136E−03	1.27
3004	103,282	103,282	40.556731	1.104E−03	1.20
3748	134,398	134,398	40.557302	5.331E−04	1.16
4507	170,850	170,850	40.557556	2.794E−04	1.12
5482	218,627	218,627	40.557696	1.395E−04	1.10
6820	276,754	276,754	40.557767	6.821E−05	1.08
8398	345,538	345,538	40.557803	3.178E−05	1.07
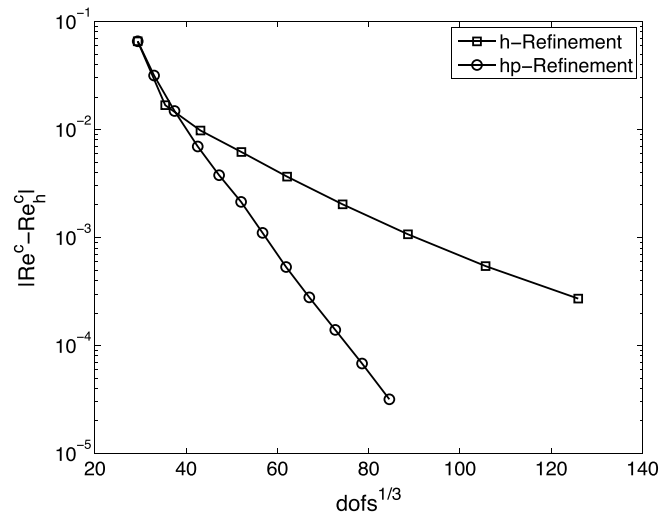
Fig. 2. 2D channel flow: comparison between *hp*- and *h*-adaptive refinement.
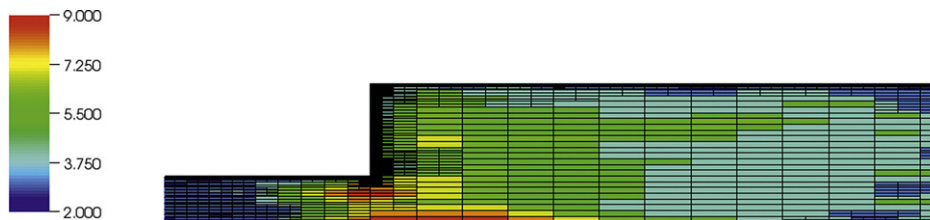
Fig. 3. 2D channel flow: *hp*-mesh after 11 adaptive refinement steps; here, the color indicates the local polynomial degree employed on each element.

In Fig. 2 we plot the results shown in Table 1; in particular, we plot the error $|Re^c - Re_h^c|$ using *hp*-refinement against the third root of the total number of degrees of freedom employed for both the base and null functions, on a linear–log scale. We see that after the initial pre-asymptotic region, the error in the computed Re_h^c using *hp*-refinement becomes a straight line, thereby indicating exponential convergence. Furthermore, in Fig. 2 we plot the true error in the computed Re_h^c using *h*-refinement, cf. [2]; here, we clearly observe the superiority of the adaptive *hp*-refinement algorithm. Indeed, on the final mesh the true error in the computed Re_h^c using *hp*-refinement is over an order of magnitude smaller than the error $|Re^c - Re_h^c|$ when *h*-refinement is employed alone.

Finally, in Fig. 3 we show the resultant *hp*-mesh after 11 adaptive refinement steps. We notice that *h*-refinement has been employed in the vicinity of the re-entrant corner, as we would expect, with *p*-enrichment being exploited elsewhere within the interior of the channel domain, where the underlying solution is expected to be smooth.

5.2. Flow in a cylindrical pipe with a stenotic region

In this second example we consider a cylindrical pipe of diameter D with an axisymmetric stenotic region of axial length L and radius $r(z)$, given by $r(z) = (D_{min} + (D - D_{min})\sin^2(\pi z L))/2$, $-1/2 \leq z/L \leq 1/2$, where z denotes the coordinate
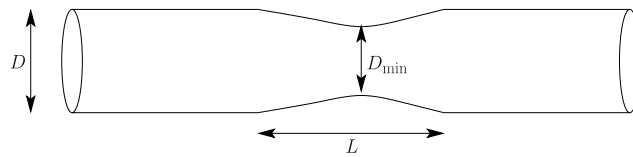
Fig. 4. Stenosis domain.

Table 2
3D flow through a pipe with a stenotic region: hp-adaptive algorithm; see [9].

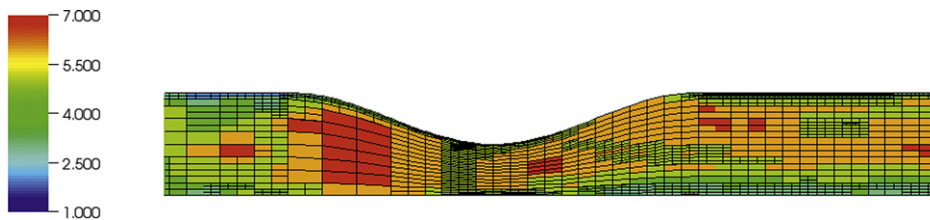| Eles	Base dof	Null dof	Re_h^c	$|Re^c - Re_h^c|$	$|\sum_{\kappa \in \mathcal{T}_h} \eta_\kappa|$	τ
3,840	84,480	119,040	662.66203	58.390	67.559	1.16
6,498	146,362	206,090	708.96275	12.090	11.296	0.93
7,512	193,518	271,480	716.36055	4.692	4.680	1.00
9,576	259,439	363,362	721.02371	2.881E−02	3.575E−02	1.24
10,101	327,537	456,501	721.05195	5.710E−04	8.054E−04	1.41
10,788	398,569	553,522	721.05247	5.477E−05	5.477E−05	1.00

Fig. 5. 3D flow through a pipe with a stenotic region: hp-mesh after 5 adaptive refinement steps; here, the color indicates the local polynomial degree employed on each element. See [9].

direction along the pipe, centered in the middle of the stenosis, see Fig. 4. The stenosis degree S is given by $S = 1 - (D_{\min}/D)^2$; here, we consider the case when $S = 0.75$, with the stenosis length $L/D = 2$. In the case when a Poiseuille flow profile is specified at the inlet, with this configuration, it is known that a steady $O(2)$ symmetry breaking bifurcation occurs with azimuthal wave number $m = 1$ when $Re^c \approx 721.0527$, cf. [24,25,13,11]. In Table 2, see also the conference article [9], we show the performance of our adaptive algorithm based on employing 5 hp-refinements. Here, the effectivity indices are close to unity on all of the adaptive meshes employed, indicating that the computed error representation formula again provides a reliable estimate for the error in the computed critical Re. Fig. 5 shows the resultant hp-mesh after 5 adaptive refinement steps. We notice that refinement has been carried out primarily downstream from the stenosis near the wall of the pipe, although some further refinement has also been performed upstream from the stenosis. In particular, we observe that h-refinement has occurred mainly near the boundary of computational domain, as well as in the center of the stenosis, while p-refinement has been utilized elsewhere.

Finally, in Fig. 6 we plot the results shown in Table 2 on a linear–log scale, together with a comparison with an adaptive strategy employing only h-refinement. As in the previous example, we again observe that after the initial pre-asymptotic region, the error in the computed Re_h^c using hp-refinement becomes a straight line, thereby indicating exponential convergence. Furthermore, on the final mesh the true error in the computed Re_h^c using hp-refinement is almost four orders of magnitude smaller than the corresponding quantity when h-refinement is employed, for the same number of degrees of freedom.

5.3. Flow in a cylindrical pipe with a spherical blockage

In our third example we consider a cylindrical pipe of radius R_1, blocked by a sphere of radius R_2, centered on the axis of symmetry of the pipe with $R_1 : R_2 = 2 : 1$, cf. Fig. 7. Fine grid computations indicate that the symmetric steady solution becomes unstable at the critical Reynolds number $Re^c \approx 359.36696$, cf. [11].

The performance of the hp-adaptive algorithm is demonstrated in Table 3; here, we notice that there is a degradation in the quality of the effectivity indices, in the sense that some over/under estimation by the computed error representation formula is now evident. In Fig. 8 we again compare the performance of our proposed hp-adaptive refinement strategy with a standard h-refinement algorithm exploiting only mesh subdivision. As in the previous examples, we again observe the superiority of employing the former refinement strategy, when compared to h-refinement; indeed, the error in the computed Re_h^c is over three orders of magnitude smaller when hp-refinement is employed in comparison to the same quantity computed using h-adaptivity.

The plot of the hp-mesh after 7 adaptive refinement steps is shown in Fig. 9. We notice that a significant amount of refinement has been carried out upstream of the blockage (although more has been performed downstream), cf. [11]. In
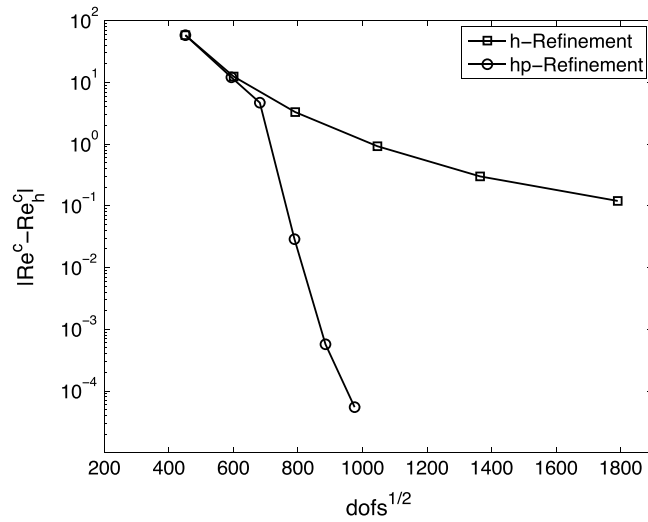
Fig. 6. 3D flow through a pipe with a stenotic region: comparison between *hp*- and *h*-adaptive refinement; see [9].
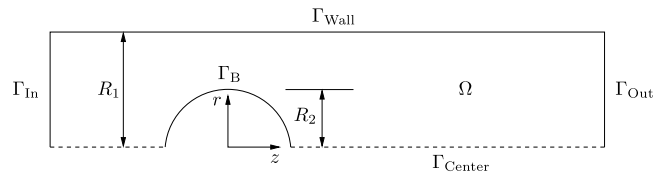

Fig. 7. Cylindrical pipe with a spherical blockage.

Table 3
3D flow through a pipe with a spherical blockage: *hp*-adaptive algorithm.

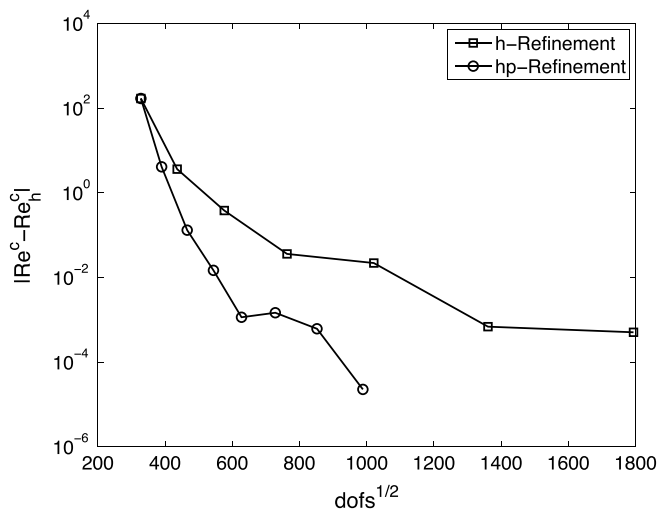| Eles	Base dof	Null dof	Re_h^c	$|Re^c - Re_h^c|$	τ
2032	44,704	62,992	528.8505	1.695E+02	2.10
2572	63,216	88,804	363.4804	4.115	1.21
3367	90,343	126,619	359.4966	1.311E−01	0.51
4177	123,363	172,489	359.3506	1.480E−02	1.09
4789	164,534	229,231	359.3643	1.151E−03	3.53
5644	221,985	308,302	359.3639	1.473E−03	0.51
6307	304,605	421,407	359.3648	6.150E−04	0.45
6550	411,377	566,644	359.3654	2.276E−05	0.99

Fig. 8. 3D flow through a pipe with a spherical blockage: comparison between *hp*- and *h*-adaptive refinement.
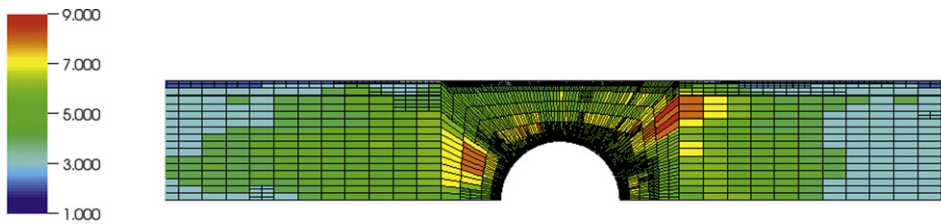
Fig. 9. 3D flow through a pipe with a spherical blockage: *hp*-mesh after 7 adaptive refinement steps; here, the color indicates the local polynomial degree employed on each element.

Table 4
3D flow through a pipe with a sudden expansion: *hp*-adaptive algorithm.

Eles	Base dofs	Null dofs	Re_h^c	$\left|\sum_{\kappa \in \mathcal{T}_h} \eta_\kappa\right|$
15,517	232,755	325,857	4925.51	211.880
17,989	311,300	434,264	4708.29	342.372
24,523	448,495	624,696	4996.91	85.547
18,730	844,468	1,158,267	5084.79	1.663
19,411	995,544	1,363,010	5084.95	7.869E−02

particular, local mesh subdivision has been undertaken in the vicinity of the boundary of the computational domain, whereas local polynomial degree enrichment has been exploited elsewhere.

5.4. Flow in a cylindrical pipe with a sudden expansion

In this final example we investigate the stability of axisymmetric flows in a cylindrical pipe with a sudden expansion, with inlet to outlet ratio of $R_1 : R_2$. At the inlet we assume Poiseuille flow. This problem represents the three-dimensional generalization of the two-dimensional channel with a sudden expansion presented in Section 5.1. While the two-dimensional problem is well-documented from both an experimental and computational point of view, the bifurcation structure of the three-dimensional analogue considered in this section still remains poorly understood. Experimental work undertaken in [12], for the case $R_1 : R_2 = 1 : 2$, has revealed that a steady symmetric flow becomes asymmetric at Reynolds number $Re^c = 1139 \pm 10$, and the resulting steady asymmetric flow is stable until the onset of time dependence at $Re^c = 1453 \pm 41$. However, the computational work undertaken in [11] indicates the onset of instability at $Re^c \approx 5080 \pm 5$; these computational results were attained using an *h*-adaptive refinement algorithm, with a total of 5.9 M degrees of freedom.

The purpose of this section is to undertake this computationally difficult problem with *hp*-adaptivity in order to compute Re^c to high accuracy. To this end, in Table 4 we show the number of elements, the number of degrees of freedom in computing the primal base solution and the primal null function, the value of Re_h^c, and the computed error representation formula $\left|\sum_{\kappa \in \mathcal{T}_h} \eta_\kappa\right|$; note that effectivities are not reported, since a sufficiently accurate reference value for Re^c is not available for this problem. From Table 4, we determine that $Re^c \approx 5084$; indeed, our computational results would indicate that four digits of accuracy have been attained for the numerical approximation to the critical Reynolds number Re^c. Moreover, compared with the *h*-adaptive results reported in [11], greater accuracy has been achieved using only 2.4 M degrees of freedom. A comparison of Re_h^c with the total number of degrees of freedom employed in the underlying finite element space when both *h*- and *hp*-refinement are employed is shown in Fig. 10.

Finally, as in [11], we remark that there is a large discrepancy between the numerical results presented in both the current article and [11] with the experimental results; we refer to [11] for further discussion of this issue.

6. Concluding remarks

This article has been devoted to the application of high-order *hp*-adaptive DGFEMs for the computation of the critical Reynolds number Re^c in the numerical approximation of the two- and three-dimensional incompressible Navier–Stokes equations in the case when the underlying system possesses either reflectional Z_2 symmetry or both rotational and reflectional $O(2)$ symmetry, respectively. Here, reliable goal-oriented *a posteriori* estimates of the error in the computed Re^c have been developed, based on employing the DWR framework in the context of *hp*-version DGFEM approximations of the associated bifurcation problem. Numerical experiments for standard test cases have been undertaken which clearly highlight the superiority of the proposed *hp*-adaptive refinement strategy when compared to standard mesh subdivision strategies (*h*-refinement). The application of these ideas to the challenging problem of flow through a cylindrical pipe with a sudden expansion has also been undertaken. In this setting, reliable estimates of the critical Reynolds number have been computed which provide more accurate predictions to those computed utilizing only *h*-refinement for a fixed polynomial
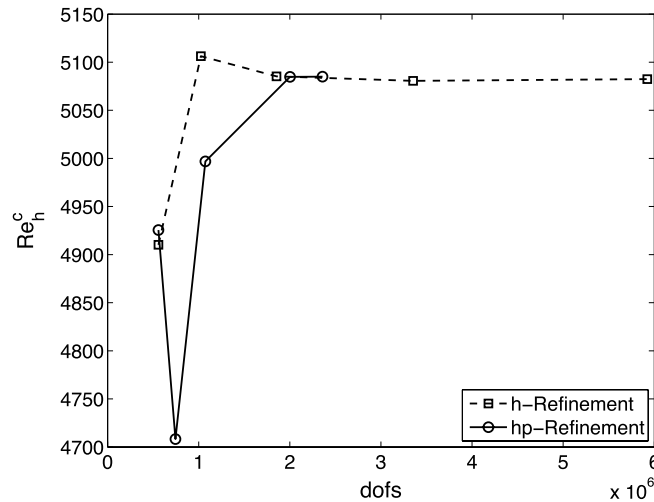
Fig. 10. 3D flow through a pipe with a sudden expansion: comparison between *hp*- and *h*-adaptive refinement.

degree. However, significant work is still required to fully understand this problem and in particular to shed light on the different predictions of Re^c computed numerically and experimentally.

References

 [1] K.A. Cliffe, A. Spence, S. Tavener, $O(2)$-symmetry breaking bifurcation: with application to the flow past a sphere in a pipe, Internat. J. Numer. Methods Fluids 32 (2000) 175–200.
 [2] K.A. Cliffe, E.J.C. Hall, P. Houston, E. Phipps, A. Salinger, Adaptivity and a posteriori error control for bifurcation problems II: incompressible fluid flow in open systems with Z_2 symmetry, J. Sci. Comput. 47 (2011) 389–418.
 [3] F. Brezzi, J. Rappaz, P. Raviart, Finite dimensional approximation of non-linear problems III, simple bifurcation points, Numer. Math. 38 (1981) 1–30.
 [4] B. Werner, A. Spence, The computation of symmetry-breaking bifurcation points, SIAM J. Numer. Anal. 21 (1984) 388–399.
 [5] D. Arnold, F. Brezzi, B. Cockburn, L. Marini, Unified analysis of discontinuous Galerkin methods for elliptic problems, SIAM J. Numer. Anal. 39 (2001) 1749–1779.
 [6] B. Cockburn, G. Kanschat, D. Schötzau, C. Schwab, Local discontinuous Galerkin methods for the Stokes system, SIAM J. Numer. Anal. 40 (2002) 319–343.
 [7] B. Cockburn, G. Kanschat, D. Schötzau, The local discontinuous Galerkin method for the Oseen equations, Math. Comp. 73 (2004) 569–593.
 [8] R. Becker, R. Rannacher, An optimal control approach to a-posteriori error estimation in finite element methods, in: A. Iserles (Ed.), Acta Numerica, Cambridge University Press, 2001, pp. 1–102.
 [9] K.A. Cliffe, E.J.C. Hall, P. Houston, Application of *hp*-adaptive discontinuous Galerkin methods to bifurcation phenomena in pipe flows, in: A. Cangiani, R. Davidchack, E. Georgoulis, A. Gorban, J. Levesley, M. Tretyakov (Eds.), Numerical Mathematics and Advanced Applications, ENUMATH 2011, Springer, 2013, pp. 333–340.
[10] K.A. Cliffe, E.J.C. Hall, P. Houston, E. Phipps, A. Salinger, Adaptivity and a posteriori error control for bifurcation problems I: the Bratu problem, Commun. Comput. Phys. 8 (2010) 845–865.
[11] K.A. Cliffe, E.J.C. Hall, P. Houston, E. Phipps, A. Salinger, Adaptivity and a posteriori error control for bifurcation problems III: incompressible fluid flow in open systems with $O(2)$ symmetry, J. Sci. Comput. 52 (2012) 153–179.
[12] T. Mullin, J. Seddon, M. Mantle, A. Sederman, Bifurcation phenomena in the flow through a sudden expansion in a circular pipe, Phys. Fluids 21 (2009).
[13] K.A. Cliffe, E.J.C. Hall, P. Houston, Adaptive discontinuous Galerkin methods for eigenvalue problems arising in incompressible fluid flows, SIAM J. Sci. Comput. 31 (2010) 4607–4632.
[14] M. Golubitsky, D. Schaeffer, Singularities and Groups in Bifurcation Theory, Vol. I, Springer, New York, 1985.
[15] M. Golubitsky, I. Stewart, D. Schaeffer, Singularities and Groups in Bifurcation Theory, Vol. II, Springer, New York, 1988.
[16] A. Vanderbauwhede, Local Bifurcation and Symmetry, Pitman, 1982.
[17] P. Aston, Analysis and computation of symmetry-breaking bifurcation and scaling laws using group theoretic methods, SIAM J. Math. Anal. 22 (1991) 139–152.
[18] K.A. Cliffe, A. Spence, S. Tavener, The numerical analysis of bifurcation problems with application to fluid mechanics, in: A. Iserles (Ed.), Acta Numerica, vol. 9, Cambridge University Press, 2000, pp. 39–131.
[19] P. Houston, E. Süli, A note on the design of *hp*-adaptive finite element methods for elliptic partial differential equations, Comput. Methods Appl. Mech. Engrg. 194 (2–5) (2005) 229–243.
[20] P.R. Amestoy, I.S. Duff, J. Koster, J.Y. L'Excellent, A fully asynchronous multifrontal solver using distributed dynamic scheduling, SIAM J. Matrix Anal. Appl. 23 (2001) 15–41.
[21] P.R. Amestoy, I.S. Duff, J.Y. L'Excellent, Multifrontal parallel distributed symmetric and unsymmetric solvers, Comput. Methods Appl. Mech. Eng. 184 (2000) 501–520.
[22] P.R. Amestoy, A. Guermouche, J.Y. L'Excellent, S. Pralet, Hybrid scheduling for the parallel solution of linear systems, Parallel Comput. 32 (2006) 136–156.
[23] R. Fearn, T. Mullin, K.A. Cliffe, Nonlinear flow phenomena in a symmetric sudden expansion, J. Fluid Mech. 211 (1990) 595–608.
[24] S. Sherwin, H. Blackburn, Three-dimensional instabilities and transition of steady and pulsatile axisymmetric stenotics flows, J. Fluid Mech. 533 (2005) 297–327.
[25] H. Blackburn, S. Sherwin, D. Barkley, Convective instability and transient growth in steady and pulsatile stenotic flows, J. Fluid Mech. 607 (2008) 267–277.